

PAPER

View Article Online
View Journal | View IssueCite this: *Dalton Trans.*, 2019, **48**,
4299Tuning the properties of tris(hydroxypyridinone)
ligands: efficient ^{68}Ga chelators for PET imaging†Cinzia Imberti,  ^a Yu-Lin Chen, ^b Calum A. Foley, ^a Michelle T. Ma,  ^a
Brett M. Paterson,  ^{‡a,c} Yifu Wang, ^a Jennifer D. Young, ^a Robert C. Hider ^b and
Philip J. Blower  ^{*,a}

The prototype tris(1,6-dimethyl-3-hydroxypyridin-4-one) chelator for gallium-68, THP^{Me}, has shown great promise for rapid and efficient kit-based ^{68}Ga labelling of PET radiopharmaceuticals. Peptide derivatives of THP^{Me} have been used to image expression of their target receptors *in vivo* in preclinical and clinical studies. Herein we describe new synthetic routes to the THP platform including replacing the 1,6-dimethyl-3-hydroxypyridin-4-one N¹–CH₃ group of THP^{Me} with O (tris(6-methyl-3-hydroxypyran-4-one, THPO) and N¹–H (tris(6-methyl-3-hydroxypyridin-4-one), THP^H) groups. The effect of these structural modifications on lipophilicity, gallium binding and metal ion selectivity was investigated. THP^H was able to bind ^{68}Ga in extremely mild conditions (5 min, room temperature, pH 6, 1 μM ligand concentration) and, notably, *in vivo*, when administered to a mouse previously injected with ^{68}Ga acetate. The ^{67}Ga radio-labelled complex was stable in serum for more than 7 days. [$^{68}\text{Ga}(\text{THP}^{\text{H}})$] displayed a log *P* value of -2.40 ± 0.02 , less negative than the log *P* = -3.33 ± 0.02 measured for [$^{68}\text{Ga}(\text{THP}^{\text{Me}})$], potentially due to an increase in intramolecular hydrogen bonding attributable to the N¹–H pyridinone units. Spectrophotometric determination of the Ga³⁺/Fe³⁺ complex formation constants for both THP^{Me} and THP^H revealed their preference for binding Ga³⁺ over Fe³⁺, which enabled selective labelling with $^{68}\text{Ga}^{3+}$ in the presence of a large excess of Fe³⁺ in both cases. Compared to THP^{Me}, THP^H showed significantly reduced affinity for Fe³⁺, increased affinity for Ga³⁺ and improved radiolabelling efficiency. THPO was inferior to both THP^H and THP^{Me} in terms of labelling efficiency, but its benzylated precursor Bn-THPO (tris(6-methyl-3-benzoyloxy-pyran-4-one)) provides a potential platform for the synthesis of a library of THP compounds with tunable chemical properties and metal preferences.

Received 8th November 2018,
Accepted 11th February 2019

DOI: 10.1039/c8dt04454f

rsc.li/dalton

Introduction

Positron emission tomography (PET) is a non-invasive clinical diagnostic technique to visualise molecular processes *in vivo*. Gallium-68 (^{68}Ga) has become a popular radionuclide for PET imaging, due to its favourable decay properties, generator-based availability and convenient half-life (68 min).^{1–3} Most ^{68}Ga PET imaging exploits peptides labelled with ^{68}Ga *via* an appropriate bifunctional chelator, to target specific disease-related receptors. ^{68}Ga -DOTATATE, ^{68}Ga -DOTATOC and ^{68}Ga -DOTANOC, all

of which contain peptides targeting the somatostatin receptor type II (SSTR2), have become clinical standards for imaging neuroendocrine tumours,⁴ while ^{68}Ga -PSMA, containing a Glu-urea-Lys moiety targeting the prostate-specific membrane antigen (PSMA, glutamate carboxypeptidase II) shows great promise for prostate cancer imaging in clinical trials.^{5,6}

An attractive attribute of ^{68}Ga is that, in principle, bifunctional chelators that bind gallium rapidly and with high affinity could be used for single-step kit-based radiolabelling, minimising handling of radioactivity and avoiding difficult, time-consuming radiosynthesis and purification steps.⁷ For optimal efficiency and convenience at the point of use it is important to minimise reaction time, radiation dose to operators and dependency on costly automated synthesis equipment. Therefore, an ideal chelator for ^{68}Ga must (i) bind Ga³⁺ in mild conditions, without need for pre-processing of the ^{68}Ga generator eluate or purification of the radiolabelled complex; (ii) give complexes of high kinetic/thermodynamic stability that are resistant to *in vivo* transchelation; and (iii) produce a single well-defined radiolabelled species. Because

^aKing's College London, School of Biomedical Engineering and Imaging Sciences, St Thomas' Hospital, London SE1 7EH, UK. E-mail: Philip.Blower@kcl.ac.uk, Cinzia.Imberti@kcl.ac.uk

^bKing's College London, School of Biomedical Sciences, Institute of Pharmaceutical Science, London, SE1 9NH UK

^cUniversity of Melbourne, School of Chemistry, Melbourne, VIC 3010, Australia

†Electronic supplementary information (ESI) available. See DOI: 10.1039/c8dt04454f

‡Current address: Monash University, School of Chemistry, Clayton, VIC, 3800, Australia.



the concentration of $^{68}\text{Ga}^{3+}$ in generator eluates is very low, preference for Ga^{3+} over other metal contaminants in eluates or in equipment used for radiolabelling (vials, syringes *etc.*) is also important to obtain radiotracers with high molar activity.

Despite efforts to develop suitable chelators (Fig. S1†) for ^{68}Ga radiolabelling, these ideals are only very recently being approached. The tetraazacyclododecane chelator DOTA, used in several ^{68}Ga -peptide radiopharmaceuticals, requires harsh radiolabelling conditions (low pH, high temperature) not compatible with sensitive biomolecules, and long reaction times unsuitable for the 68 min half-life of ^{68}Ga .^{8,9} The triazacyclononane chelator NOTA and its phosphinic acid derivatives of the TRAP family represent an advance on DOTA, often providing quantitative radiochemical yield (RCY) at room temperature and acidic pH.^{8,10,11} The “chimeric” DATA chelators, possessing both cyclic and an acyclic nitrogen atoms, can be radiolabelled quantitatively with ^{68}Ga over a wide pH range and resist demetallation in the presence of transferrin or Fe^{3+} .^{12,13} For all these chelators, radiolabelling with ^{68}Ga is hampered particularly by the presence of Cu^{2+} .^{13–15} Zn^{2+} also competes with Ga^{3+} for coordination to NOTA and DATA ligands.^{15,16} The acyclic chelator H_2dedpa was radiolabelled with ^{68}Ga at room temperature and acidic pH, achieving high molar activities.¹⁷

Another class of Ga^{3+} ligands with potential to meet the above ideals is based on siderophores and iron chelators, exploiting the similarity between Ga^{3+} and Fe^{3+} in terms of charge, ionic radius (62 pm for Ga^{3+} vs. 65 pm for high spin Fe^{3+} (ref. 18)) and preference for hard oxygen donors. The siderophore fusarinine-C (FSC),¹⁹ obtained from the fungus *Aspergillus fumigatus*, showed excellent ^{68}Ga radiolabelling giving high molar activity over a wide (3–8) pH range. The bacterial siderophore deferoxamine (DFO-B) can also be radiolabelled with ^{68}Ga in a wide pH range, but is subject to metal dissociation at low concentration²⁰ and cannot compete effectively with other ^{68}Ga chelators.²¹ The acyclic HBED (*N,N*-bis(2-hydroxybenzyl)ethylenediamine-*N,N*-diacetic acid), employed in a ^{68}Ga PSMA tracer,²² binds gallium(III) and iron(III) with very high affinity ($\log K_{\text{Ga}} = 37.73$, $\log K_{\text{Fe}} = 36.74$).²³ The tris(hydroxypyridinone) chelator THP^{Me} (Fig. 1, previously known as CP256 and $\text{THP}^{24–31}$), investigated as a ^{68}Ga chelator, was also initially developed as an iron-chelating agent.³² It has a tripodal scaffold supporting three pendant 3-hydroxypyridin-4-one (HP) units based on the bidentate chelating drug deferi-

prone (Fig. 1). Each arm can coordinate Ga^{3+} through the deprotonated hydroxyl and carbonyl groups.³³ THP^{Me} is an efficient gallium chelator, out-competing other popular chelators²¹ and achieving quantitative radiolabelling in extremely mild conditions without eluate pre-processing or post-labelling purification,²⁴ to produce a single [$^{68}\text{Ga}(\text{THP}^{\text{Me}})$] species, unlike other chelators such as HBED.²¹ Bifunctional derivatives based on THP^{Me} -amine conjugates (Fig. 1) have been used to produce several peptide and protein conjugates, with promising results. These include peptides targeting the SSTR2,²⁶ $\alpha_v\beta_3$ integrin,²⁷ the prostate specific membrane antigen (PSMA)²⁸ and small proteins.³⁴ The PSMA-targeting THP^{Me} conjugate is now in phase 2 trials and routine clinical use in some centres.^{30,35–37} A dendrimer derivative of THP^{Me} (HP9) has also been developed to achieve higher molar activity ^{68}Ga -bioconjugates.²⁹

While ^{68}Ga - THP^{Me} -PSMA was comparable to its HBED counterpart in PET imaging of tumours,²⁸ other derivatives such as the ^{68}Ga - THP^{Me} -TATE and ^{68}Ga - THP^{Me} -RGD₃ demonstrated a lower tumour/non-target organ ratio compared to ^{68}Ga radiotracers based on DOTA chelators,^{27,31} revealing how different targets may benefit from chelators with different chemical properties and, in turn, the potential value of structural variants on this promising platform. Another potential concern (albeit not arising in practice so far) is that similarity between Fe^{3+} and Ga^{3+} may lead to competition with adventitious Fe^{3+} (from vials, syringe needles radiolabelling equipment or generator eluate). Further optimisation of THP ligand design is therefore important. Modification at the ring nitrogen offers a straightforward way to tailor THP properties such as lipophilicity and hydrogen bonding capability. Previous studies on bidentate hydroxypyridinone ligands show that modification at the ring nitrogen is possible without significant detriment to their M^{3+} affinity.^{33,38}

Herein we present new synthetic routes to THP ligands, including the new derivative THP^{H} (Scheme 1) in which the *N*-methyl groups have been replaced by hydrogen. The labelling efficiency and lipophilicity of [$^{68}\text{Ga}(\text{THP}^{\text{H}})$] is compared to its THP^{Me} and tris(hydroxypyranone) (THPO) analogues, and the conditional formation constants of the Ga^{3+} and Fe^{3+} complexes are evaluated, to measure and improve upon the gallium-selectivity and effectiveness of the prototype THP^{Me} for ^{68}Ga radiolabelling.

Results and discussion

Synthesis

Synthesis of the precursor Bn-HP^H (**4**, Scheme 1) from **1** was first attempted using the previously reported approach to THP^{Me} synthesis³⁹ (Scheme 1, **strategy A**), *i.e.*, conversion of **1** into pyridinone **2** by reaction with ammonia, followed by a Mitsunobu reaction with phthalimide and subsequent deprotection of the newly-introduced nitrogen with hydrazine at reflux. The Mitsunobu reaction failed to give the desired product, likely due to competition by the $\text{N}^1\text{-H}$ group with the

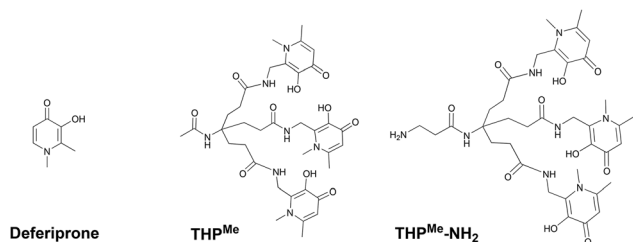
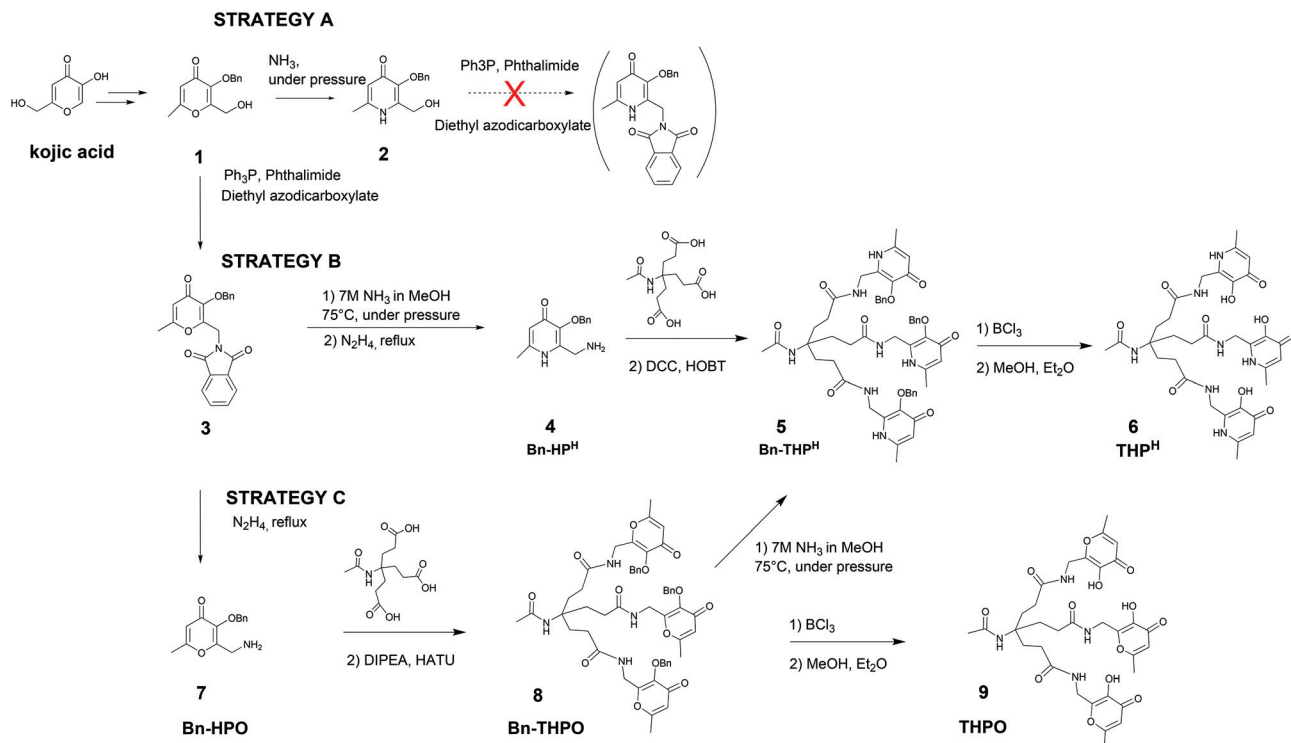


Fig. 1 Hydroxypyridinone-based chelators. Left to right: Prototype bidentate ligand deferiprone; hexadentate ligand THP^{Me} ; $\text{THP}^{\text{Me}}\text{-NH}_2$, the basis of bifunctional derivatives.





Scheme 1 Synthetic pathways evaluated for synthesis of THP^H and its tris(hydroxypyranone) counterpart THPO.

phthalimide N–H group for deprotonation and subsequent S_N2 reaction on the phosphonium-activated alcohol. New synthetic strategies were therefore developed.

In **strategy B**, the Mitsunobu reaction was performed directly on **1** (to avoid deleterious side reactions of the pyridinone N¹–H group). The pyranone–pyridinone conversion was then carried out on **3**, followed by deprotection of the NH₂ functionality to give the new primary amine-containing hydroxypyridinone, Bn-HP^H (**4**). This was coupled with the tripodal tricarboxylic acid³² to give Bn-THP^H (**5**) in 15.6% overall yield.

In an alternative approach (**strategy C**), the pyranone–pyridinone conversion was performed after assembling the hexadentate tripodal unit. Compound **3** was deprotected to give the hydroxypyranone bearing a pendant primary amine, Bn-HPO (**7**), which was then coupled to the tricarboxylic acid to obtain the benzyl-protected tris(hydroxypyranone) Bn-THPO (**8**). Treatment of **8** with ammonia under pressure to give Bn-THP^H (**5**) was monitored using LC-MS (Fig. 2). The overall yield of Bn-THP^H (**5**) from compound **1** *via strategy C* (7.3%), was lower than that *via strategy B*, due to the additional step. However, in **strategy C** the benzylated tris(hydroxypyranone) precursor Bn-THPO holds great promise as a flexible platform for synthesising a versatile library of tris(hydroxypyridinone) compounds with varying substituents at the pyridyl nitrogen, by reaction with a large excess of the relevant primary amine. The LC-MS data show that the pyranone-to-pyridinone conversion proceeded in a step-wise fashion, offering the opportunity to create mixed species containing both pyranone and pyridinone units, or mixed pyridinone units.

Debenzylation of Bn-THP^H (**5**) with BCl₃ produced the desired chelator THP^H (**6**) quantitatively. The same deprotection procedure applied to Bn-THPO (**8**) gave the tris(6-methyl-3-hydroxypyran-4-one) chelator THPO (**9**) in 78% yield.

⁶⁸Ga radiolabelling and comparison with THP^{Me} and THPO

THP^H, THP^{Me} and THPO were radiolabelled at decreasing ligand concentrations in the same mild conditions (5 min, pH 6, room temperature) previously employed for THP^{Me}.²⁴ Radiochemical yields (RCY) are reported in Table 1 and compared graphically in Fig. 3.

Efficient (>95%) radiolabelling of THP^H achieved at concentrations as low as 1 μM (Table 1), was verified by iTLC and HPLC analysis. At a ligand concentration as low as 0.1 μM THP^H was still able to bind ⁶⁸Ga in 93.9% RCY while the RCY for THP^{Me} decreased to 83%, highlighting improved radiolabelling efficiency for the new chelator.

As was the case for [⁶⁸Ga(THP^{Me})], no pre-processing of the generator eluate or post-labelling purification was required to obtain a radiochemically pure complex. iTLC showed only one species, corresponding to the radiolabelled complex without the presence of colloidal or unchelated “free” ⁶⁸Ga. Analytical reversed-phase HPLC of the radiolabelling mixture (method 3) showed only one signal in the UV-Vis chromatogram (3 min 26 s), attributed to excess ligand, and one in the radiochromatogram at 4 min 56 s attributed to [⁶⁸Ga(THP^H)]. HPLC analysis of non-radioactive [^{nat}Ga(THP^H)] also showed a single peak in the UV-Vis chromatogram, whose retention time (4 min 20 s) matched that of



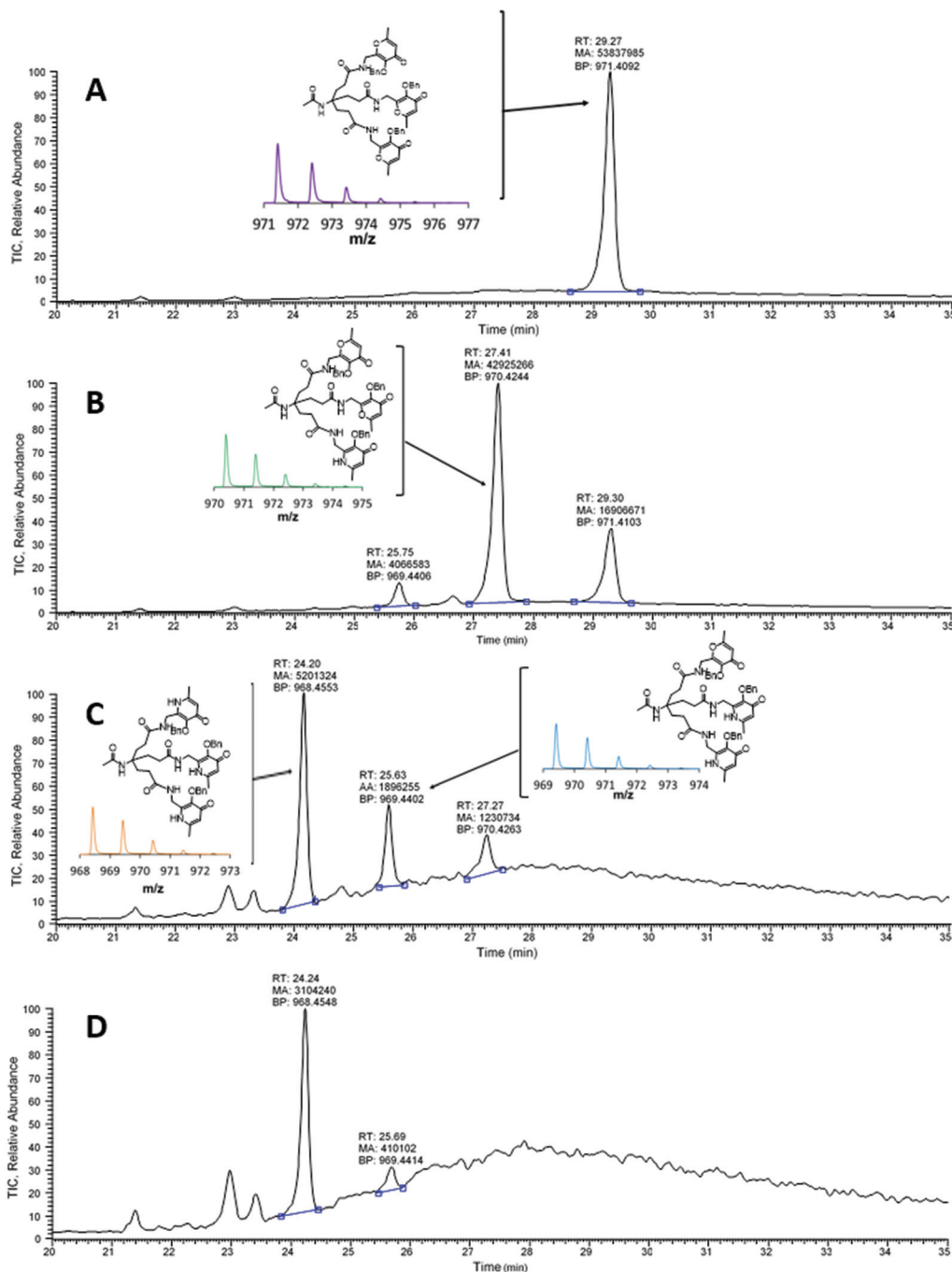


Fig. 2 LC-MS analysis (total ion current) of the reaction mixture for conversion of Bn-THPO (**8**) to Bn-THP^H (**5**) (strategy C) at (A) 0 h (B) 8 h (C) 48 h and (D) 72 h. RT: Retention time; MA: area; BP: *m/z* value. Insets: Bn-THPO and MS signal of [Bn-THPO + H]⁺ (purple), mono-substituted Bn-THPO and MS signal (green), di-substituted Bn-THPO and MS signal (blue), Bn-THP^H structure and MS signal (orange).

[⁶⁸Ga(THP^H)] after correcting for delay due to the serial configuration of the detectors (Fig. 4A). The mass spectrum of [^{nat}Ga(THP^H)] confirmed the 1:1 stoichiometry of the complex (Fig. S4†), and no other gallium-containing ions were observed. As was the case for [Ga(THP^{Me})], low solubility of [^{nat}Ga(THP^H)] prevented further characterisation by ¹H/⁷¹Ga NMR. Synthesis of more soluble conjugates of the ligands is underway to enable NMR studies.

The tris(hydroxypyranone) ligand THPO was also radio-labelled quantitatively, in the same conditions except that significantly higher ligand concentration (100 μM) was required to reach quantitative radiolabelling (Table 1). HPLC analysis (method 4) revealed a single peak at 8 min 18 s, matching the UV peak of [^{nat}Ga(THPO)] at 7 min 42 s (Fig. 4B).

The observed decreased efficiency in gallium binding was not unexpected for pyranone derivatives, whose lower electron



Table 1 Log *P* and log *D*_{7.4} values and RCY, at different ligand concentrations, of ⁶⁸Ga complexes (average ± standard deviation (*N* = 4 for log *P* and log *D*_{7.4}, *N* = 3 for RCY))

	[Ga(THP ^{Me})]	[Ga(THP ^H)]	[Ga(THPO)]
Log <i>P</i>	−3.33 ± 0.02	−2.40 ± 0.02	−1.64 ± 0.01
Log <i>D</i> _{7.4}	−3.27 ± 0.02	−2.28 ± 0.05	−1.65 ± 0.03
Radiochemical yield			
100 μM	96.9 ± 1.0	98.9 ± 0.7	95.6 ± 0.2
10 μM	97.8 ± 0.5	99.1 ± 0.2	83.0 ± 0.4
1 μM	96.7 ± 0.2	98.1 ± 0.4	27.5 ± 0.7
0.1 μM ^a	83.0 ± 0.5	93.9 ± 0.4	N/A

^a Radiolabelling performed with ⁶⁸Ga eluate from a second E&Z generator, eluted with clinical grade HCl.

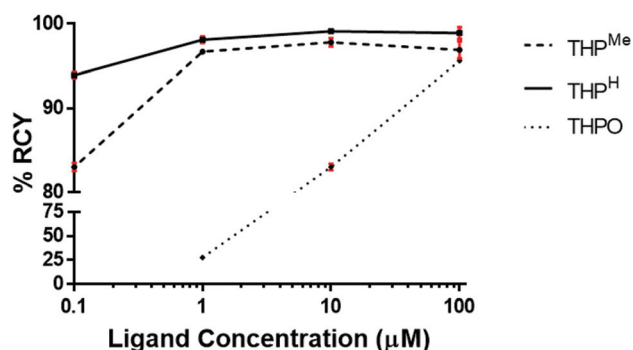


Fig. 3 Comparison of RCY (average ± standard deviation, *N* = 3) obtained by ⁶⁸Ga radiolabelling of THP^H, THP^{Me} and THPO at decreasing ligand concentration.

density of the heterocyclic ring compared to the pyridinone analogues is known to compromise binding to iron.^{32,40}

Determination of the partition and distribution coefficients (log *P* and log *D*_{7.4}, Table 1) for the ⁶⁸Ga complexes of THP^{Me} and THP^H ligands revealed, unexpectedly, higher lipophilicity of [Ga(THP^H)] than of [Ga(THP^{Me})], although both complexes were highly hydrophilic. This could be due to [Ga(THP^H)] forming intramolecular hydrogen bonds rather than hydrogen bonds with the solvent. This phenomenon was previously reported for their bidentate analogues and some amido-3-hydroxypyridin-4-one ligands.^{41–43} As expected, [Ga(THPO)], in which oxygen replaces the heterocyclic amine, was more hydrophobic than its pyridinone counterparts. This agrees with the above LC-MS results for Bn-THPO and Bn-THP^H, where sequential replacement of the 3 oxygen atoms with N¹-H groups progressively reduced retention times.

Serum stability and *in vivo* studies

The stability of a radiolabelled chelate in biological environments is critical to its utility in radiotracers. [⁶⁷Ga(THP^H)] stability in human serum was determined by size-exclusion HPLC, comparing the elution profile of the complex with that of unchelated ⁶⁷Ga in serum. The longer half-life ⁶⁷Ga was used instead of ⁶⁸Ga, to allow more prolonged evaluation of stability. [⁶⁷Ga(THP^H)] was stable in serum for at least 8 days

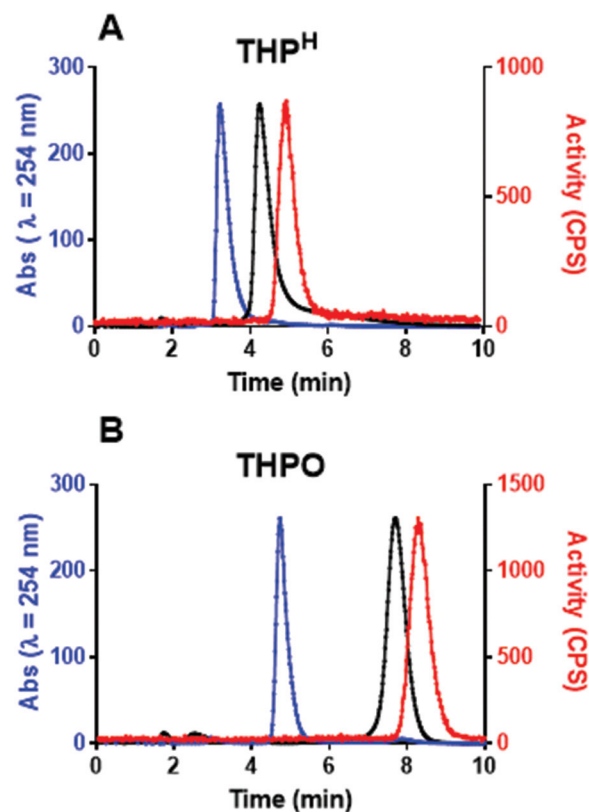


Fig. 4 Normalised chromatograms of THP^H (A) and THPO (B) and their gallium complexes. Blue: UV (254 nm) for ligand; Black: UV (254 nm) for ^{nat}Ga complex; Red: radiochromatogram for ⁶⁸Ga complex. The serial configuration of the detectors accounts for a 36 seconds delay between UV and radio-chromatograms.

with no shift in its chromatographic signal (retention time: 15 min 30 s) compared to the complex incubated in PBS. When unchelated ⁶⁷Ga was incubated in serum, by contrast, ⁶⁷Ga eluted at 12 min at early serum incubation time points (chelated as ⁶⁷Ga EDTA by EDTA in the mobile phase, Fig. S7†), but became more associated with serum proteins over time: after 8 days incubation two new signals appeared, at 12 min [⁶⁷Ga(EDTA)] and 9 min 30 s (serum proteins). Excellent serum stability has been previously observed for [⁶⁷Ga(THP^{Me})], which showed no sign of transchelation after 4 h at 37 °C.²⁴

A preliminary evaluation of the behaviour and stability of [⁶⁸Ga(THP^H)] *in vivo* was performed. PET imaging of a SCID beige mouse injected with [⁶⁸Ga(THP^H)] revealed rapid renal excretion (Fig. 5A). Reversed-phase HPLC of urine at 60 min post injection revealed a single radioactive species, corresponding to intact [⁶⁸Ga(THP^H)] (4.9 min, Fig. 5B). A similar biodistribution has been reported for [Ga(THP^{Me})].²⁴

The ability of THP^H to scavenge gallium *in vivo* was also investigated. Fig. 6 shows how ⁶⁸Ga biodistribution in a mouse injected with acetate-buffered ⁶⁸Ga³⁺ suddenly changed upon injection of the chelator: most of the activity previously in the blood pool cleared quickly from the blood into the kidneys and the bladder (Fig. 6A). HPLC analysis of urine confirmed



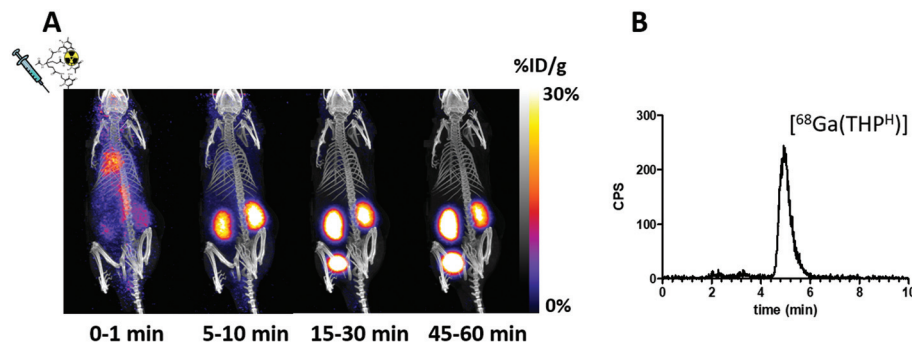


Fig. 5 (A) Dynamic PET/CT MIP in a mouse injected with $[^{68}\text{Ga}(\text{THP}^{\text{H}})]$. Fast blood clearance is evident, with only kidneys and bladder visible in the 15–30 min image. (B) radioHPLC of urine 60 min after injection (method 3), showing a single peak attributed to $[^{68}\text{Ga}(\text{THP}^{\text{H}})]$ (Fig. 4A).

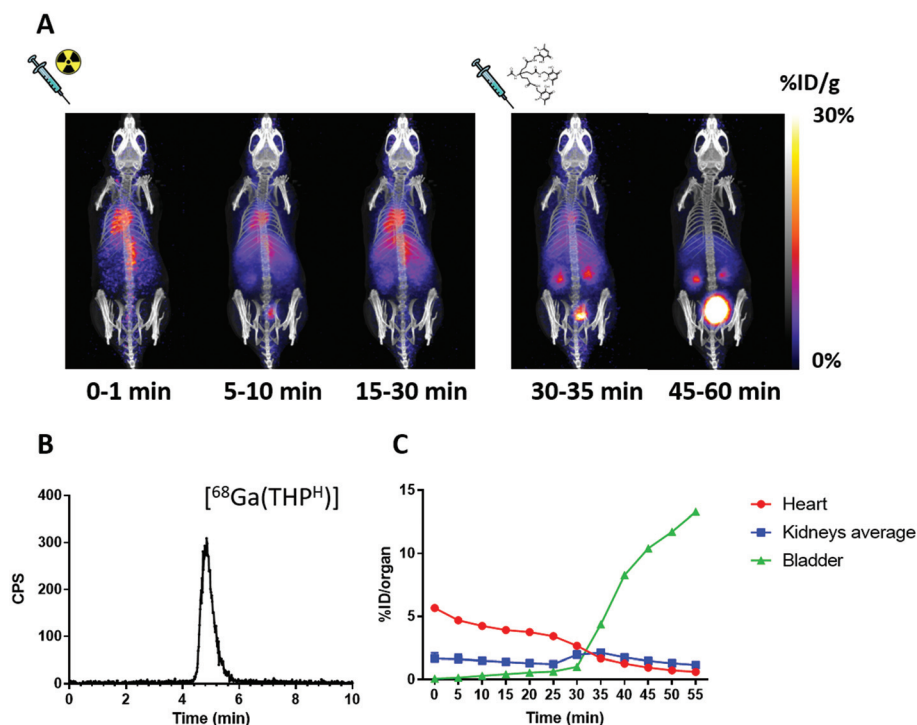


Fig. 6 (A) Dynamic PET/CT MIP of a mouse injected with acetate buffered ^{68}Ga at time 0 followed by THP^{H} at 30 min. Blood clearance of ^{68}Ga acetate (represented by radioactivity in the heart ventricles) is slow in the first 30 min. After the injection of THP^{H} a sudden clearance occurs through the kidneys into the bladder. (B) RadioHPLC of urine 60 min after ^{68}Ga injection (method 3), showing only one peak, attributed to $[^{68}\text{Ga}(\text{THP}^{\text{H}})]$. (C) Time/activity curves showing % ID in heart (as a measure of blood activity), kidneys and bladder as a function of time. Each data point represents a 5 min interval defined by its starting time.

in vivo radiolabelling of the chelator (Fig. 6B), showing one peak corresponding to $[^{68}\text{Ga}(\text{THP}^{\text{H}})]$. This scavenging ability, shared with THP^{Me} (ESI, Fig. S8†), reflects the rapid complexation kinetics and the extraordinary ability to transchelate gallium (which is known to bind rapidly and almost completely to transferrin when intravenously injected⁴⁴) rapidly in the biological milieu.

Spectrophotometric determination of conditional formation constants

The THP^{Me} and THP^{H} acid dissociation and conditional formation constants for their Ga^{3+} and Fe^{3+} complexes were

investigated by spectrophotometric measurements. pK_{a} and pM values (defined as $-\log[\text{M}^{3+}]$ when $[\text{ligand}]_{\text{total}} = 10 \mu\text{M}$, $[\text{metal}]_{\text{total}} = 1 \mu\text{M}$ and $\text{pH} = 7.4$) are reported in Table 2. A full list of the measured conditional formation constants is provided in the ESI (Tables S1–S3†), together with speciation plots calculated for the pH range of the titration. The pK_{a} values for THP chelators are better described as intrinsic protonation constants since they represent the average pK_{a} values of the three hydroxypyridinone units, which could not be distinguished by UV spectrophotometric measurements.⁴⁵ The first intrinsic pK_{a} is attributed to the carbonyl group of the HP unit, and the second to the adjacent hydroxyl group.



Table 2 Acid dissociation and conditional Fe^{3+} and Ga^{3+} complex formation constants for THP^{Me} and THP^{H} . Estimated overall error for each value <3%. pM values were calculated based on $[\text{M}]_{\text{total}} = 1 \mu\text{M}$, $[\text{L}]_{\text{total}} = 10 \mu\text{M}$ and $\text{pH} = 7.4$

	THP^{Me}	THP^{H}	Deferiprone ^a
$\text{pK}_{\text{a}1}$	3.2 ^b	3.4 ^b	3.5
$\text{pK}_{\text{a}2}$	9.4 ^b	9.5 ^b	9.8
$\text{pK}_{\text{a}3}$	N/A	13.0 ^c	N/A
pFe	29.1	28.6	20.8
pGa	30.0	31.8	20.7

^a Previously reported measurements on deferiprone³³ were repeated here to confirm the reliability of our titration method. ^b Intrinsic pK_{a} values⁴⁵ were determined from spectrophotometric titration. When deviation from the obtained intrinsic pK_{a} values were considered (± 0.2 – 0.8 log units), no significant changes in pM values (less than 3%) were observed. ^c Estimated pK_{a} value. No significant spectral change was observed between pH 11.5 and 12.5 for pK_{a} titration. Changing the estimated pK_{a} value can result in different metal log β values for THP^{H} but no appreciable change in pM values.

For THP^{H} a third intrinsic protonation constant, $\text{pK}_{\text{a}3}$, associated with deprotonation of the $\text{N}^1\text{--H}$ group in the pyridinone ring, exists outside the pH range used. The value of $\text{pK}_{\text{a}3}$ was estimated to be 13 from the spectral change of the $[\text{Fe}(\text{THP}^{\text{H}})]$ complex in the pH 10–12.5 range. The measured protonation constants for THP^{H} are lower than those measured for deferiprone, but slightly higher than those for THP^{Me} (that is, THP^{Me} is slightly more acidic than THP^{H}). This was unexpected considering the presence of electron-donating *N*-methyl group and suggests that other chemical interactions (e.g. hydrogen bonding) may be influencing the pK_{a} of these compounds.

The data in Table 2 show that THP^{H} has higher affinity than THP^{Me} for Ga^{3+} but, unexpectedly, lower than THP^{Me} for Fe^{3+} . The conditional formation constants indicate that both THP^{H} and THP^{Me} are selective for Ga^{3+} over Fe^{3+} . This was unexpected considering that deferiprone lacks a preference for either metal,³³ implying that the tripodal scaffold is critical in determining the coordination preferences of these hexadentate chelators.

Achievement of thermodynamic equilibrium for Ga^{3+} and Fe^{3+} complex formation/dissociation is a relatively slow process.²³ Therefore, traditional spectrophotometric and potentiometric techniques, which allow only a few minutes equilibration, may produce apparent stability constants harbouring a kinetic component. In contrast, batch titrations, with equilibration over several days/weeks, generally result in more accurate “true” equilibrium stability constants. This discrepancy was recently acknowledged by Notni *et al.* for $[\text{Ga}(\text{TRAP-Pr})]$.⁴⁶ In the case of THP chelators, no significant changes in the absorbance spectra were observed beyond the equilibration period, suggesting that equilibrium had been reached, although changes after longer intervals cannot be excluded. In any case, the use of a short equilibration time is particularly relevant for radiopharmaceutical applications, where radiolabelling processes must be rapid.

Competition experiments

To quantify the preference of the two ligands for Ga^{3+} over Fe^{3+} in a radiolabelling setting, a competition experiment was performed, where ^{68}Ga radiolabelling of THP^{Me} and THP^{H} in the presence of different concentrations of Fe^{3+} was investigated. Instead of a traditional “no-carrier-added” radiolabelling mixture, in these competition studies non-radioactive $^{\text{nat}}\text{Ga}^{3+}$ was added to ^{68}Ga eluate (to reach a gallium:ligand ratio of approx. 9:10 to introduce competition by ensuring that the ligand concentration was sufficient to bind just one of the two metals quantitatively). Since ^{68}Ga is chemically indistinguishable from natural gallium and its addition negligibly increases the total concentration of Ga^{3+} , the percentage of $^{68}\text{Ga}^{3+}$ bound to the ligand reflects the percentage of total Ga^{3+} bound to the ligand. To ensure constant pH at different metal concentrations, a higher concentration of ammonium acetate buffer than in conventional radiolabelling experiments was necessary (final concentration 0.44 M). Upon addition of the THP ligand (≈ 1 equivalent, 10 μM) to mixtures of $^{\text{nat}}/^{68}\text{Ga}^{3+}$ (0.9 equivalent) and Fe^{3+} (0, 0.9 or 9 equivalents) the radiochemical yield of the radiolabelling mixture was measured by iTLC (mobile phase 2) at different time points (Fig. 7).

Unexpectedly, under these conditions (unlike conventional radiolabelling conditions) THP^{Me} could not reach quantitative radiochemical yield even in the absence of iron, probably because the higher buffer and metal salt concentration increases the abundance of competing ligands (ammonia, acetate, nitrate) compared to more conventional labelling media. Nonetheless, it is clear that despite the presence of insufficient ligand to bind all the Ga^{3+} and Fe^{3+} , the ^{68}Ga -labelling efficiency was not dramatically reduced by the presence of even a ten-fold excess (compared to ligand) of Fe^{3+} . Notably, the presence of 0.9 equivalents of iron with 0.9 of gallium decreased the radiochemical yield for the two ligands only marginally (not significantly for either ligand at later time points, $p = 0.06$ for THP^{Me} , $p = 0.22$ for THP^{H}), indicating that iron could not compete effectively with gallium for ligand binding. When the amount of iron was increased to 9 equivalents (a ten-fold excess over gallium), still the majority of the ligand bound to Ga^{3+} and not Fe^{3+} , indicating a clear preference of THP ligands for gallium over iron (≈ 40 fold preference for gallium over iron under these conditions was estimated considering that a $\approx 80:20$ gallium:iron complex ratio prevailed when a 10 fold excess of iron over gallium was present). This strong preference of both THP^{Me} and THP^{H} for binding Ga^{3+} over Fe^{3+} indicates that the presence of significant amounts of iron should not adversely affect the performance of the chelators during radiolabelling or *in vivo*.

A second competition study between THP^{Me} and THP^{H} was conducted, to determine whether their different affinities for gallium would affect their relative ^{68}Ga labelling efficiency. The difference in retention factor between the two complexes on iTLC (mobile phase 1) was exploited to monitor a solution in which ^{68}Ga was added to an equimolar mixture of the two ligands (100 μM each, with equimolarity ensured by inte-



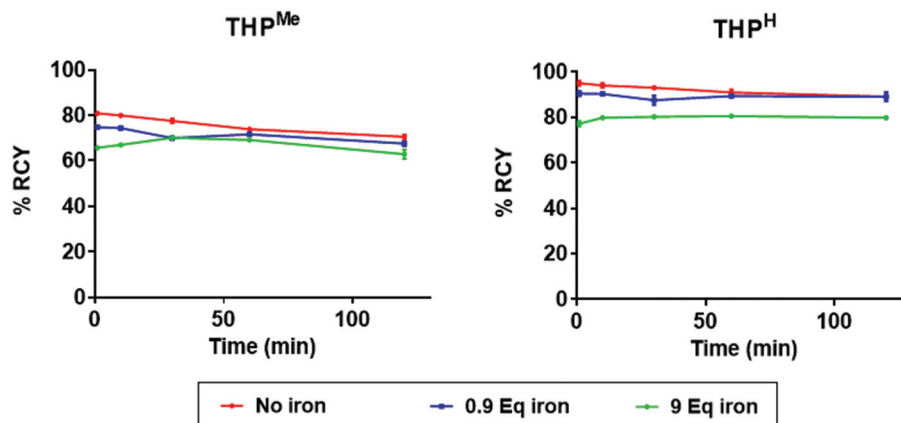


Fig. 7 Influence of various concentrations of Fe^{3+} on the radiochemical yield of $[^{68}\text{Ga}(\text{THP}^{\text{Me}})]$ and $[^{68}\text{Ga}(\text{THP}^{\text{H}})]$ in the presence of 1 equivalent of ligand ($10\ \mu\text{M}$) and 0.9 equivalent of $^{\text{nat}}\text{Ga}^{3+}$ (average \pm standard deviation; for control samples (without Fe) $N = 6$, for other samples $N = 3$ (error bars are too small to be visible).

gration of the ^1H NMR spectrum, Fig. S6†), by sampling at different times after the addition (Fig. 8). After one minute the radioactivity was already quantitatively chelated, indicating extremely fast radiolabelling for both compounds, but with preference for THP^H (ratio: 70 : 30). By 120 min the ratio had increased to $\approx 90 : 10$, confirming that gallium binds preferentially to THP^H rather than THP^{Me}. These data agree qualitatively with the spectrophotometric measurements and suggest that binding to both ligands is initially under kinetic control, while the thermodynamic preference for THP^H is established by 30 min. Interestingly, these results also demonstrate that

Ga^{3+} can transchelate from THP^{Me} to THP^H under these conditions. While this suggests a degree of kinetic lability of the $[\text{Ga}(\text{THP})]$ system when excess ligand is present, resistance towards transchelation *in vivo* (where excess ligand is greatly diluted) has been extensively confirmed in previous preclinical and clinical studies,^{24,26–30} including the present manuscript (Fig. 5).

Both spectrophotometric titration and competition experiments show how modification at the hydroxypyridinone ring unexpectedly influences the preference of THP chelators for Ga^{3+} vs. Fe^{3+} , whereas a similar effect was not observed for

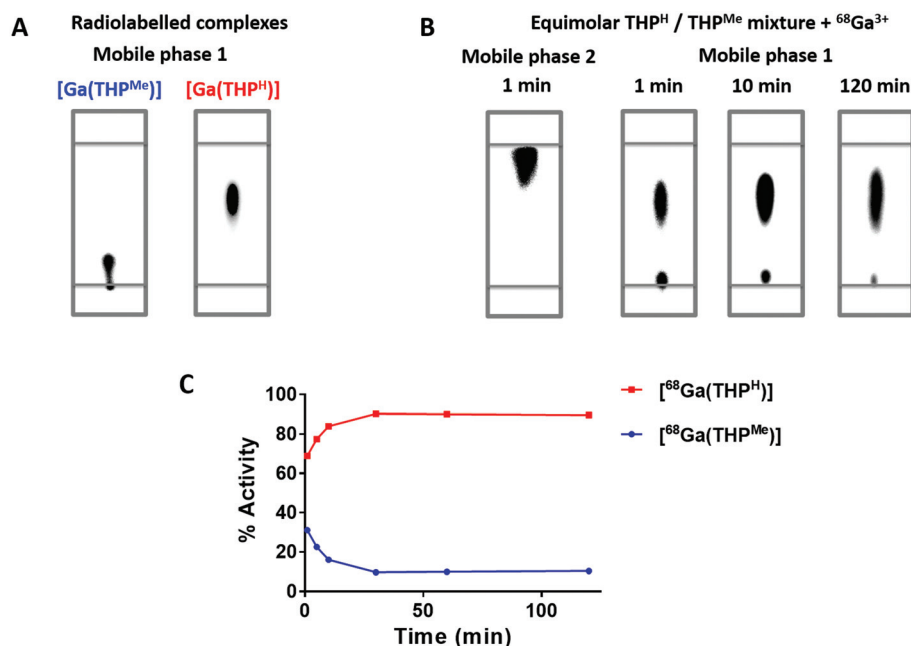


Fig. 8 iTLCs of the radioactive ^{68}Ga complexes of THP^{Me} and THP^H in mobile phase 1 (A) and of an equimolar mixture of THP^{Me} and THP^H treated with $^{68}\text{Ga}^{3+}$ in mobile phase 2 (1 min time point) or in mobile phase 1 (1, 10 and 120 min) (B), imaged with a phosphorimager. (C) Shows how the percentage of activity associated with the two chelators, as calculated from the images, changes over time. Data are average \pm standard deviation ($N = 3$, error bars are too small to be visible).



bidentate hydroxypyridinone compounds.³⁸ This implies that geometric restrictions imposed by the tripodal structure of the ligand are critical to metal ion selectivity. It is likely that replacing the *N*¹-methyl group with hydrogen modifies the steric constraints and the degree and type (*e.g.* intramolecular *vs.* intermolecular) of hydrogen bonding, compared to THP^{Me}. Both these factors could result in marked changes in the geometry and rigidity of the coordination sphere, leading to different metal affinities and selectivity of the two THP chelators.

Conclusions

Despite the acyclic topology of THP^{Me} and THP^H, their affinity for Ga³⁺ is very high (pGa = 30.0 and 31.8 respectively) and, contrary to our naive expectation, exceeds their affinity for Fe³⁺. The reasons for this preference are unknown, but likely related to geometry constraints imposed by the tripodal framework, since no such preference was observed for the bidentate chelator deferiprone.³³ An important consequence of this selectivity is that the expected vulnerability of the THP ligands to competition with iron, during labelling and *in vivo*, is not manifested either in the measurements described here or in the preclinical and clinical uses of THP^{Me} described so far.^{24,26–30,35–37} Moreover, minor alteration of the hydroxypyridinone moiety (replacing *N*¹-CH₃ with *N*¹-H) significantly improves both the affinity for Ga³⁺ (and hence ⁶⁸Ga radiolabelling efficiency) and the selectivity for Ga³⁺ over Fe³⁺ (and hence resistance to interference from adventitious iron). The origin of this effect may be related to changes in intramolecular hydrogen bonding, which affect the ability of the scaffold to provide an idealised octahedral cavity of appropriate size, for as yet unknown reasons. Synthesis of more soluble derivatives is underway to allow investigation of these factors by NMR. As well as producing THP^H as a new tris(hydroxypyridinone) ligand with superior Ga³⁺-chelating properties compared to the established THP^{Me}, we have described a novel synthetic strategy that allows further systematic modification of pyridinone nitrogen substituents by using the protected THPO as a common precursor. This opens the door to further tuning of ligand design to improve labelling efficiency and modify biological behaviour.

Experimental section

Materials and instrumentation

Chemicals were obtained from Sigma Aldrich, unless otherwise specified, and used without further purification. NMR spectra were acquired on a Bruker Advance 400 spectrometer with a 5 mm Quattro Nucleus Probe (QNP) at 400.13 MHz. Chemical shifts are referenced to the appropriate solvent peak. Positive ion mass spectra were recorded using an Agilent 6510 QTOF spectrometer. Analytical reversed-phase LC-MS were acquired on a Thermo Scientific Exactive Orbitrap Mass

Spectrometer coupled to a Thermo Scientific Accela Pump with CTC Autosampler, using a ThermoFisher HyperSil GOLD column (2.1 × 150 mm, 5 μm), flow rate 0.2 mL min⁻¹. Data were acquired and reference mass-corrected *via* a dual-spray electrospray ionisation source, using the factory-defined calibration procedure. Semi-preparative HPLC was carried out using an Agilent Eclipse XDB-C18 column (9.4 × 250 mm, 5 μm), flow rate 3 mL min⁻¹, and UV detection at 214 nm on an Agilent 1200 LC system. Mobile phase A was water with 0.1% TFA and mobile phase B was acetonitrile with 0.1% TFA. For method 1, concentration of B increased from 0 to 100% at 1% min⁻¹. For method 2, concentration of B increased from 20% to 100% in 100 min. Analytical reversed-phase HPLC was performed on the same system using an Agilent Eclipse XDB-C18 column (4.6 × 150 mm, 5 μm) with a 1 mL min⁻¹ flow rate and UV detection at 214 or 254 nm, coupled to a LabLogic Flow-Count radioactivity detector with a sodium iodide probe (B-FC-3200). Mobile phase A was water with 0.1% TFA, mobile phase B was acetonitrile with 0.1% TFA. For methods 3 and 4, UV detection was set at 254 nm and isocratic elution was used with 10% B and 15% B, respectively. For methods 5 and 6, UV detection was set at 214 nm and gradients included 5 min of equilibration at 0% B at the start of the run. For method 5, concentration of B increased from 0% (at 5 min) to 45% (at 15 min) and subsequently decreased to 0 (at 20 min). For method 6, % B increased from 0% (at 5 min) to 75% (15 min) and back to 0% (20 min). Size-exclusion chromatography was conducted using a BioSep SEC-s2000 column (145 Å, 300 × 7.8 mm, 5 μm) with a mobile phase of PBS with 50 mM EDTA trisodium salt, flow rate 1 mL min⁻¹. ⁶⁸Ga was obtained from an Eckert & Ziegler ⁶⁸Ge/⁶⁸Ga-generator eluted with high-purity 0.1 M HCl (Fluka Analytical). Instant thin layer chromatography strips (iTLC-SG, Varian Medical Systems) were run in two different mobile phases (mobile phase 1: 0.1 M citrate pH 5; mobile phase 2: 1:1 ammonium acetate 2 M: methanol) and visualised using a Cyclone Plus Phosphor Imager (PerkinElmer) and a Raytest Rita-Star TLC scanner.

Synthesis and characterisation data

2-Hydroxymethyl-3-benzyloxy-6-methyl-pyran-4(1*H*)-one (**1**) was synthesised following published procedures.³⁹ THP^H was synthesised from **1** employing two different synthetic strategies using reactions based on literature methods.^{32,39} The tripodal scaffold 4-acetamido-4-(2-carboxyethyl)heptanedioic acid was synthesised following literature procedures.³² All intermediates and final products were characterised by ESI-MS, ¹H NMR and ¹³C NMR (Fig. S9–S16†).

2-Hydroxymethyl-3-benzyloxy-6-methyl-pyridin-4(1*H*)-one (**2**)

A solution of **1** (1.010 g, 4 mmol) in ethanol (5 mL) was sealed in a thick-walled glass vial containing 25% aqueous ammonia (20 mL) and stirred at 75 °C overnight. Addition of concentrated HCl to reach neutral pH precipitated white crystals, which were collected by filtration and washed with cold water and diethyl ether (0.609 g, 60.6%). ESI-MS (*m/z*): 246.12 [*M* + *H*]⁺ calcd: 246.11 for C₁₄H₁₅NO₃ + *H*⁺. ¹H NMR (methanol-*d*₄,



400 MHz) δ : 2.33 (s, 3H, C⁶-CH₃), 4.34 (d, 2H, C²-CH₂-OH), 5.08 (s, 2H, C³-O-CH₂-Ph), 6.33 (s, 1H, C⁵-H in pyridinone), 7.35 (m, 5H, C³-O-CH₂-Ph). ¹³C NMR (methanol-*d*₄, 100 MHz) δ : 18.7 (C⁶-CH₃), 57.0 (C²-CH₂-OH), 74.6 (C³-O-CH₂-Ph) 117.1 (C⁵-H in pyridinone), 128.0 (*o*-CH in benzyl), 129.4 (*p*-CH in benzyl), 130.2 (*m*-CH in benzyl), 138.6 (i-C-CH₂ in benzyl), 143.0 (C² in pyridinone), 144.7 (C³ in pyridinone), 147.8 (C⁶ in pyridinone), 176.0 (C⁴ in pyridinone).

2-Phthalimidomethyl-3-benzyloxy-6-methyl-pyran-4(1H)-one (3)

A solution of **1** (1.05 g, 4.0 mmol), triphenylphosphine (1.395 g, 8 mmol) and phthalimide (1.181 g, 8 mmol) in dry tetrahydrofuran (20 mL) under an atmosphere of nitrogen was cooled to 0 °C and diethyl azodicarboxylate (2 mL, 8 mmol) was added dropwise. After stirring overnight, methanol was added to quench excess diethyl azodicarboxylate prior to solvent removal by rotary evaporation. The white residue was recrystallised from methanol affording white crystals (1.157 g, 72.3%). **ESI-MS** (*m/z*): 376.11 [M + H]⁺, calcd: 376.12 for C₂₂H₁₇NO₅ + H⁺. ¹H NMR (DMSO-*d*₆, 400 MHz) δ : 2.14 (s, 3H, C⁶-CH₃), 4.73 (s, 2H, C²-CH₂-N), 5.10 (s, 2H, C³-O-CH₂-Ph), 6.26 (s, 1H, C⁵-H in pyranone), 7.40 (m, 5H, C³-O-CH₂-Ph), 7.89 (m, 4H, phthalimide). ¹³C NMR (DMSO-*d*₆, 100 MHz) δ : 19.0 (C⁶-CH₃), 34.4 (C²-CH₂-N), 72.9 (C³-O-CH₂-Ph), 114.3 (C⁵-H in pyranone), 123.4 (C⁷-H and C⁴-H in phthalimide), 128.2 (*o*-CH in benzyl), 128.4 (*p*-CH in benzyl), 128.5 (*m*-CH in benzyl), 131.4 (C⁵-H and C⁶-H in phthalimide), 134.7 (C^{3a} and C^{7a} in phthalimide), 136.8 (i-C-CH₂ in benzyl), 142.6 (C² in pyranone), 153.9 (C³ in pyranone), 165.1 (C⁶ in pyranone) 167.2 (C=O in phthalimide), 174.6 (C⁴ pyranone).

Bn-HP^H (2-aminomethyl-3-benzyloxy-6-methyl-pyridin-4(1H)-one) (4)

A solution of **3** (500 mg, 1.3 mmol) in 7 M ammonia solution in methanol (30 mL) was added to a thick-walled glass vial that was sealed and stirred overnight at 75 °C. Aqueous hydrazine (55%, 0.2 mL) was then added to the reaction mixture and the solution heated at reflux for 3 h. After removal of the solvent by rotary evaporation the brown residue was purified by silica-gel chromatography (CH₂Cl₂:MeOH = 80:20, *R*_f = 0.35) to afford Bn-HP^H (317 mg, 45%).

ESI-MS (*m/z*): 245.13 [M + H]⁺, calcd: 245.13 for C₁₄H₁₆N₂O₂ + H⁺. ¹H NMR (methanol-*d*₄, 400 MHz) δ : 2.33 (s, 3H, C⁶-CH₃), 3.60 (s, 2H, C²-CH₂-NH₂), 5.14 (s, 2H, C³-O-CH₂-Ph), 6.39 (s, 1H, C⁵-H in pyridinone), 7.36 (m, 5H, C³-O-CH₂-Ph). ¹³C NMR (methanol-*d*₄, 100 MHz) δ : 19.4 (C⁶-CH₃), 38.8 (C²-CH₂-NH₂), 74.6 (C³-O-CH₂-Ph) 116.7 (C⁵-H in pyridinone), 129.6 (*o*-CH in benzyl), 129.6 (*p*-CH in benzyl), 130.4 (*m*-CH in benzyl), 138.5 (i-C-CH₂ in benzyl) 143.6 (C² in pyridinone), 143.8 (C³ in pyridinone), 149.0 (C⁶ in pyridinone), 174.2 (C⁴ in pyridinone).

Bn-THP^H (5) (from Bn-HP^H)

4-Acetamido-4-(2-carboxyethyl)heptanedioic acid (20 mg, 0.07 mmol), hydroxybenzotriazole hydrate (HOBT, 32.7 mg, 0.21 mmol) and dicyclohexylcarbodiimide (DCC, 44 mg,

0.21 mmol) were dissolved in the minimum amount of *N,N*-dimethylformamide (DMF, \approx 1.5 mL) and stirred. Bn-HP^H (86 mg, 0.35 mmol) was dissolved separately in 500 μ L of DMF and added to the former mixture, which was then stirred at 50 °C for 48 h. Formation of the product over time was monitored *via* LC-MS (*m/z* = 968, [M + H]⁺). DMF was removed under high vacuum and the product purified by silica gel chromatography (eluent CH₃OH:CHCl₃ = 20:80 *R*_f = 0.25, followed by CH₃OH:CHCl₃:40% aqueous NH₃ = 20:80:2) to obtain Bn-THP^H (37 mg, 48%). **ESI-MS** (*m/z*): 968.45 [M + H]⁺, 990.44 [M + Na]⁺, calcd: 968.46 for C₅₄H₆₁N₇O₁₀ + H⁺. ¹H NMR (methanol-*d*₄, 400 MHz) δ : 1.86 (s, 3H, CH₃-CO-NH-tripod), 1.88 (m, 6H, CH₂-CH₂-CO-NH-CH₂-pyridinone), 2.09 (m, 6H, CH₂-CH₂-CO-NH-CH₂-pyridinone), 2.28 (s, 9H, C⁶-CH₃), 4.10 (s, 6H, CO-NH-CH₂-pyridinone), 5.11 (s, 6H, C³-O-CH₂-Ph), 6.31 (s, 3H, C⁵-H in pyridinone), 7.35 (m, 15H, C³-O-CH₂-Ph). ¹³C NMR (methanol-*d*₄, 100 MHz) δ : 18.8 (C⁶-CH₃), 23.6 (CH₃-CO-NH-tripod), 30.8 (CH₂-CH₂-CO-NH-CH₂-pyridinone), 31.0 (CH₂-CH₂-CO-NH-CH₂-pyridinone), 37.7 (CH₂-CH₂-CO-NH-CH₂-pyridinone), 58.9 (NHC-tripod), 74.5 (C³-O-CH₂-Ph) 117.3 (C⁵-H in pyridinone), 129.5 (*p*-CH in benzyl), 130.2 (*m*-CH in benzyl), 138.5 (i-C-CH₂ in benzyl), 141.4 (C² in pyridinone), 144.8 (C³ in pyridinone), 148.0 (C⁶ in pyridinone), 173.0 (C⁴ in pyridinone), 176.1 (CH₂-CH₂-CO-NH-CH₂-pyridinone).

THP^H (6)

Bn-THP^H (17 mg, 0.018 mmol) was dissolved in the minimum amount of methanol (\approx 100 μ L) and diluted to 1 mL with dichloromethane. An excess of BCl₃ (3 mL of a 1 M solution in dichloromethane) was added through a cannula (Cole-Parmer) under an atmosphere of N₂. After 2 hours, the vial was placed on ice and excess methanol was added to quench remaining BCl₃. Volatiles were removed by rotary evaporation. The residue was redissolved in methanol and precipitated by addition of cold diethyl ether to give THP^H (3-HCl salt) (15.6 mg, 90% yield). **ESI-MS** (*m/z*): 698.32 [M + H]⁺, 349.67 [M + 2H]²⁺, 233.44 [M + 3H]³⁺, calcd: 698.31 for C₃₃H₄₃N₇O₁₀ + H⁺. ¹H NMR (D₂O, 400 MHz) δ : 1.85 (s, 3H, CH₃-CO-NH-tripod), 1.87 (m, 6H, CH₂-CH₂-CO-NH-CH₂-pyridinone), 2.17 (m, 6H, CH₂-CH₂-CO-NH-CH₂-pyridinone), 2.47 (s, 9H, C⁶-CH₃), 4.44 (d, 6H, CO-NH-CH₂-pyridinone), 6.93 (s, 3H, C⁵-H in pyridinone). ¹³C NMR (D₂O, 100 MHz) δ : 17.9 (C⁶-CH₃), 22.6 (CH₃-CO-NH-tripod), 28.9 (CH₂-CH₂-CO-NH-CH₂-pyridinone), 29.2 (CH₂-CH₂-CO-NH-CH₂-pyridinone), 36.6 (CH₂-CH₂-CO-NH-CH₂-pyridinone), 58.0 (NHC-tripod), 111.7 (C⁵-H in pyridinone), 136.4 (C² in pyridinone), 140.6 (C³ in pyridinone), 146.7 (C⁶ in pyridinone), 160.9 (C⁴ in pyridinone), 173.3 (CH₃-CO-NH-tripod), 176.4 (CH₂-CH₂-CO-NH-CH₂-pyridinone). **HPLC**: a single peak was detected using both HPLC methods 3 (λ = 254 nm, 3 min 26 s, Fig. 4A) and 5 (λ = 214 nm, 10 min 45 s, Fig. S2†).

Bn-HPO (2-(aminomethyl)-3-(benzyloxy)-6-methyl-4H-pyran-4-one) (7)

A solution of **3** (499 mg, 1.33 mmol) was dissolved in ethanol (5 mL) and heated at reflux for 3 h after addition of 5.5% of



aqueous hydrazine (1.5 mL). The pH was adjusted to 1 with concentrated HCl (37%) and the flask cooled to 0 °C. The phthalhydrazide precipitate was filtered out and the filtrate was evaporated to dryness. The resulting residue was dissolved in water (2 mL) and the pH was adjusted to 10 using concentrated NaOH (10 M). The solution was extracted with dichloromethane (4 × 2 mL), the organic layers were combined and the solvent removed by rotary evaporation. The crude product was purified by silica gel chromatography (dry loading, CH₂Cl₂ : MeOH = 90 : 10, *R_f* = 0.45) to obtain Bn-HPO (90.0 mg, 28% yield). **ESI-MS** (*m/z*): 246.11 [M + H]⁺, calcd: 246.11 for C₁₄H₁₅NO₃ + H⁺. **¹H NMR** (methanol-*d*₄, 400 MHz) δ: 2.31 (s, 3H, C⁶-CH₃), 3.51 (s, 2H, C²-CH₂-NH₂), 5.09 (s, 2H, C³-O-CH₂-Ph), 6.27 (s, 1H, C⁵-H in pyranone), 7.37 (m, 5H, C³-O-CH₂-Ph). **¹³C NMR** (methanol-*d*₄, 400 MHz) δ: 19.5 (C⁶-CH₃), 39.3 (C²-CH₂-NH₂), 74.9 (C³-O-CH₂-Ph) 115.0 (C⁵-H in pyridinone), 129.6 (*o*-CH in benzyl), 129.7 (*p*-CH in benzyl), 130.4 (*m*-CH in benzyl), 137.9 (i-C-CH₂ in benzyl) 142.3 (C² in pyranone), 162.9 (C³ in pyranone), 167.9 (C⁶ in pyranone), 178.4 (C⁴ in pyranone).

Bn-THPO (8)

The tripodal acid 4-acetamido-4-(2-carboxyethyl)heptanedioic acid (14 mg, 0.049 mmol), diisopropylethylamine (25.6 μL, 0.15 mmol) and HATU (55.7 mg, 0.15 mmol) were dissolved in the minimum volume of *N,N*-dimethylacetamide (DMA, ~500 μL), combined while stirring and left at room temp. for 1 h. A solution of Bn-HPO (52 mg, 0.16 mmol) in DMA (500 μL) was then added and the mixture stirred for 72 h. The DMA was removed under high vacuum and the product was purified using preparative HPLC (method 1) to obtain **Bn-THPO** (34.7 mg, 73.1% yield). **ESI-MS** (*m/z*): 486.21 [M + 2H]²⁺, 971.41 [M + H]⁺, 993.38 [M + Na]⁺, calcd: 971.41 for C₅₄H₅₈N₄O₁₃ + H⁺. **¹H NMR** (methanol-*d*₄, 400 MHz) δ: 1.91 (s, 3H, CH₃-CONH-tripod), 1.96 (m, 6H, CH₂-CH₂-CONH-CH₂-pyranone), 2.17 (m, 6H, CH₂-CH₂-CONH-CH₂-pyranone), 2.29 (s, 9H, C⁶-CH₃), 4.23 (s, 6H, CONH-CH₂-pyranone), 5.12 (s, 6H, C³-O-CH₂-Ph), 6.28 (s broad, 3H, C⁵-H in pyranone), 7.35 (m, 15H, C³-O-CH₂-Ph). **¹³C NMR** (methanol-*d*₄, 100 MHz) δ: 19.5 (C⁶-CH₃), 23.5 (CH₃-CO-NH-tripod), 30.9 (CH₂-CH₂-CO-NH-CH₂-pyranone), 31.2 (CH₂-CH₂-CO-NH-CH₂-pyranone), 37.3 (CH₂-CH₂-CO-NH-CH₂-pyranone), 58.9 (NHC-tripod), 75.0 (C³-O-CH₂-Ph) 115.2 (C⁵-H in pyridinone), 129.6 (*p*-CH in benzyl), 130.2 (*m*-CH in benzyl), 138.1 (i-C-CH₂ in benzyl), 143.7 (C² in pyranone), 159.1 (C³ in pyranone), 167.9 (C⁶ in pyranone), 172.9 (C⁴ in pyranone), 175.7 (CH₃-CO 169.4), 178.2 (CH₂-CH₂-CO-NH-CH₂-pyridinone).

Bn-THP^H (5) (from Bn-THPO)

Bn-THPO (22.4 mg, 0.023 mmol) was added to 7 M ammonia in MeOH (11 mL) and the mixture stirred at 75 °C in a sealed thick glass vial. The reaction was left for 72 h and monitored *via* LC-MS (mobile phase: A = H₂O + 0.1% formic acid, B = acetonitrile + 0.1% formic acid; gradient: 0–5 min 100% A, 5–55 min from 100% A to 100% B, flow rate 0.2 mL min⁻¹, mass range 900–1100 *m/z*). The solvent was then removed

under reduced pressure and the residue purified by preparative HPLC (method 2) to give Bn-THP^H (10.88 mg, 49% yield).

THPO (9)

To Bn-THPO (6.65 mg, 0.007 mmol) in DCM:MeOH (7 : 1), BCl₃ (3 mL of a 1 M solution in dichloromethane) was added *via* a cannula under a N₂ atmosphere. After 2 h, the vial was placed on ice, the reaction was quenched with MeOH and the solvent was removed under reduced pressure. The residue was dissolved in water:acetonitrile (60 : 40) and purified by preparative HPLC (method 1) to give THPO (TFA salt, 5.6 mg, 78% yield). **ESI-MS** (*m/z*): 702.26 [M + H]⁺, 723.24 [M + Na]⁺, 351.13 [M + 2H]²⁺, calcd: 701.27 for C₃₃H₄₁N₄O₁₃ + H⁺. **¹H NMR** (methanol-*d*₄, 400 MHz) δ: 1.91 (s, 3H, CH₃-CO-NH-tripod), 1.99 (t, 6H, CH₂-CH₂-CO-NH-CH₂-pyranone), 2.22 (t, 6H, CH₂-CH₂-CO-NH-CH₂-pyranone), 2.30 (s, 9H, C⁶-CH₃), 4.40 (d, 6H, CO-NH-CH₂-pyranone), 6.24 (s, 3H, C⁵-H in pyranone). **¹³C NMR** (methanol-*d*₄, 100 MHz) δ: 19.7 (C⁶-CH₃), 23.5 (CH₃-CO-NH-tripod), 31.0 (CH₂-CH₂-CO-NH-CH₂-pyranone), 31.3 (CH₂-CH₂-CO-NH-CH₂-pyranone), 37.3 (CH₂-CH₂-CO-NH-CH₂-pyranone), 59.0 (NHC-tripod), 112.3 (C⁵-H in pyranone), 143.5 (C² in pyranone), 148.9 (C³ in pyranone), 167.5 (C⁶ in pyranone), 173.0 (C⁴ in pyranone), 176.1 (CH₃-CO-NH-tripod), 176.4 (CH₂-CH₂-CO-NH-CH₂-pyranone). **HPLC**: A single peak was observed with both HPLC methods 4 (λ = 254 nm, retention time 4 min 43 s, Fig. 4B) and 6 (λ = 214 nm, 11 min 10 s, Fig. S3†).

Complexation with ⁶⁸Ga³⁺ and ^{nat}Ga³⁺

For all the radiolabelling experiments, an Eckert & Ziegler generator was eluted with 5 mL of high purity HCl 0.1 M (Fluka analytical) in five 1 mL fractions, whose activity was measured by a Capintec radionuclide dose calibrator. 100 μL of the highest activity fraction (15–20 MBq) were added to 100 μL of the ligand (concentration range 200–2 μM) in ammonium acetate 0.5 M. Verification of the radiolabelling was carried out after 5 min by reversed-phase HPLC (for THP^H: method 3; for THPO: method 4) and iTLC-SG with two different mobile phases, as described above (mobile phase 1: *R_f* [Ga(THP^H)] = 0.64 ± 0.02, *R_f* Ga_{colloid} = 0, *R_f* ⁶⁸Ga_{free} = 1; mobile phase 2: *R_f* [Ga(THP^H)] = 1, *R_f* ⁶⁸Ga_{free} = 0, ⁶⁸Ga_{colloid} = 0). Radiolabelling of THP^H at 0.1 μM was performed using a second E&Z generator, eluted with clinical grade 0.1 M HCl (E&Z).

The ^{nat}Ga complexes of THP^H and THPO were prepared by addition of an aqueous solution of Ga(NO₃)₃ (5 μL, 2 mg mL⁻¹, excess) to a solution of the ligand (50 μL, 150 μM) in ammonium acetate 0.2 M. After 5 min reaction time, an aliquot of the reaction mixture was applied to a reversed-phase HPLC column to confirm complex formation (for THP^H: method 3, for THPO: method 4, see Fig. 4A and B). **[Ga(THP^H)]** **ESI-MS** (*m/z*): 764.22 [M + H]⁺, 382.61 [M + 2H]²⁺, 349.66 [M – Ga + 4H]²⁺. Calcd: 764.22 for C₃₃H₄₀N₇O₁₀Ga + H⁺. The spectrum is reported in Fig. S4.† No peaks assignable to stoichiometry other than 1 : 1 were visible. Solubility of the complex in water or any other solvent was not sufficient to obtain a satisfactory NMR spectrum or X-ray-quality crystals.



Lipophilicity determination

^{68}Ga -radiolabelling of THP^{Me} , THP^{H} and THPO (200 μM in ammonium acetate 0.5 M) was performed as described above and verified by iTLC-SG. An aliquot (10 μL) of each radiolabelling mixture was then added to vials containing a pre-equilibrated mixture of octanol/water (500/490 μL) for $\log P$ measurements, or octanol/PBS (500 μL /490 μL) for $\log D_{7.4}$ measurements. The mixtures were vortexed and then shaken for 30 min before separation of the two phases by centrifugation (4000 rpm, 3 min). The activity in aliquots of each phase (20 μL aqueous phase, 100 μL octanol phase) was measured in the gamma-counter and corrected for the different volumes sampled. Each experiment was repeated 4 times.

Spectrophotometric determination of conditional formation constants

The automated titration system consists of a Metrohm 765 Dosimat autoburette, a Mettler Toledo MP230 pH meter with SENTEK pH electrode (P11), and an HP 8453 UV-visible spectrophotometer with a Hellem quartz flow cuvette, with circulation driven by a Gilson Mini-plus #3 pump (speed capability 20 mL min^{-1}). A potassium chloride electrolyte solution (0.1 M) was used to maintain the ionic strength. The temperature of the test solutions was maintained in a thermostatic jacketed titration vessel at 25 ± 0.1 $^{\circ}\text{C}$, using a Fisherbrand Isotemp water bath. The pH electrodes were calibrated using the software GLEE⁴⁷ with data obtained by titrating a volumetric standard HCl (0.1 M) in KCl (0.1 M) with KOH (0.1 M) under an atmosphere of argon. Analytical grade reagent materials were used in the preparation of all solutions. The solution under investigation was stirred vigorously during the experiment. For pK_{a} determinations, a cuvette path length of 10 mm was used, while for metal stability constants determinations, a cuvette path length of 50 mm was used (experimental concentration was *ca.* 40 μM for iron complexes and *ca.* 10 μM for gallium complexes). All instruments were interfaced to a computer and controlled by an in-house program.

The automated titration adopted the following strategy: the pH of a solution was increased in increments of 0.1 pH unit by the addition of potassium hydroxide solution (0.1 M) from the autoburette. The pH readings were judged stable if they varied by less than 0.01 pH unit after a pre-set incubation period. For pK_{a} determinations, an incubation period of 1.5 min was adopted; for metal stability constant determinations, an incubation period of 3 min was adopted. The cycle was repeated until the predefined end point pH value was achieved. Titration data were analysed with the HypSpec2014 program^{48,49} (<http://www.hyperquad.co.uk/>). The fitting spectra range for iron complexes was 400–700 nm while that for gallium complexes was 250–350 nm. pH values higher than 11.3 (outside the pH range in which electrode measurements are considered accurate) were neglected and re-calculated from the added KOH quantity (using “no pH” mode within the HypSpec2014 program). The associated hydrolysis constants used in the analysis were collected from Martell’s critical stabi-

lity constants.⁵⁰ Metal affinities of compounds in this study were determined in competition with the metal hydrolysis species in a solution at a high pH (titrated up to pH 12.5). Satisfactory fitting of the THP^{Me} titration for both iron and gallium were achieved. In contrast, the titration of THP^{H} was found to be more complex due to the presence of the additional protonation sites. A satisfactory result for the THP^{H} /gallium interaction was achieved, but not for iron, which is possibly related to different log stability constants of $[\text{Fe}(\text{OH})_4]^-$ and $[\text{Ga}(\text{OH})_4]^-$ ($\log \beta = 34.4$ and 39.4 respectively⁵⁰). Instead, the corresponding stability constant was obtained using EDTA-iron-hydroxide species competition at the high pH range following a slightly modified titration procedure (cuvette path length: 100 mm, incubation period: 30 min, experimental concentration of iron complexes: *ca.* 20 μM , experimental concentration of EDTA: *ca.* 50 mM). Speciation plots (Tables S1–S3†) were calculated with the HYSS program.⁵¹

Ligand competition for $^{68}\text{Ga}^{3+}$ binding

A solution containing both THP^{Me} and THP^{H} , each 2 mM, in D_2O was diluted to 100 μM with aqueous ammonium acetate (0.5 M) after NMR analysis had been used to confirm equal concentration of the two compounds (Fig. S5†). 50 μL of the mixture were mixed with an equal volume of ^{68}Ga eluate. The percentage of radioactivity associated with each compound was measured by iTLC-SG (mobile phase 1 and 2) at different time points (1, 5, 10, 30, 60 and 120 minutes).

Metal competition for THP binding

A standard ICP-MS solution of iron(III) in nitric acid (Alfa Aesar) was diluted in 0.1 M nitric acid (Fluka analytical) to obtain 2250 μM and 225 μM $\text{Fe}(\text{III})$ solutions. The same procedure was used to prepare a 225 μM $\text{Ga}(\text{III})$ solution from its ICP-MS standard solution (Sigma Aldrich). The $\text{Ga}(\text{III})$ solution (20 μL , 225 μM) was mixed with the $\text{Fe}(\text{III})$ solution (20 μL , 225 or 2250 μM Fe) or with 0.1 M nitric acid as a control (20 μL) and the ^{68}Ga generator eluate was added (20 μL , $[\text{Ga}^{3+}] \approx 2$ nM and was considered negligible). The relevant THP ligand (440 μL of a 11.3 μM solution in 0.5 M ammonium acetate buffer) was added to the radiolabelling mixture (final concentration: $[\text{THP}] = 10$ μM , $[\text{Ga}^{3+}] = 9$ μM , $[\text{Fe}^{3+}] = 0, 9$ or 90 μM). The radiochemical yield at different times was measured by iTLC-SG (mobile phase 2). Statistical analysis was performed using a *t*-test between the “no Fe” and “0.9 eq. Fe” groups.

$[^{67}\text{Ga}(\text{THP}^{\text{H}})]$ serum stability

^{67}Ga chloride (50 μL , 5 MBq), obtained from Nordion (Canada), was added to THP^{H} (50 μL , 100 μM) in 0.5 M ammonium acetate. Quantitative radiolabelling was verified after 5 min of incubation, *via* iTLC-SG. The retention time on a size-exclusion HPLC (mobile phase: PBS with 50 mM EDTA trisodium salt) was 15 min 30 s for $[^{67}\text{Ga}(\text{THP}^{\text{H}})]$. The retention time for ^{67}Ga chloride in the same conditions was 12 min. An aliquot of each solution (60 μL) was added to male AB human serum (600 μL , Sigma) and incubated at 37 $^{\circ}\text{C}$. Size-



exclusion radiochromatography was performed after 1 h, 1 day and 8 days incubation.

In vivo studies with THP^H

All *in vivo* experiments were carried out in accordance with British Home Office regulations governing animal experimentation and complied with guidelines on responsibility in the use of animals in bioscience research of the U.K. Research Councils and Medical Research Charities, under U.K. Home Office project and personal licences. Male SCID/beige mice (7 months old, Charles River) were used for preliminary animal studies on THP^H. Dynamic PET scanning was performed using a nanoScan® PET/CT (Mediso Medical Imaging Systems).⁵² Respiration rate and bed temperature were monitored throughout. PET/CT datasets were reconstructed using the Monte-Carlo-based full 3D iterative algorithm Tera-Tomo (Mediso Medical Imaging Systems).⁵³ All reconstructed datasets were analysed using VivoQuant 1.21 software (inviCRO), which enables the co-registration of PET and CT images and the delineation of regions of interest (ROIs) for quantification of activity in specific organs. Mice were anaesthetised with isoflurane (O₂ flow rate of 1.0–1.5 L min^{−1} and isoflurane levels of 2–2.5%) cannulated at the tail vein using a catheter (25 µL volume) and a CT scan was performed. Subsequently, a PET scan was started and the radiotracer injected. One mouse (37 g) was injected with of a [⁶⁸Ga(THP^H)] solution (307 µL, 5 µM, 6.59 MBq) and imaged for 1 hour to determine biodistribution and *in vivo* stability of the radiolabelled complex. A second mouse (33 g) was injected with acetate buffered ⁶⁸Ga (100 µL, 0.1 M ammonium acetate, 4.68 MBq), without THP^H or other chelator, while scanning, followed at 30 min by an injection of THP^H (50 µL of a 50 µM solution in PBS). Animals were then sacrificed by neck dislocation while still anaesthetised. Urine was collected and analysed by reversed-phase HPLC (method 3).

PBS	Phosphate-buffered saline
PET	Positron emission tomography
PSMA	Prostate specific membrane antigen
RCY	Radiochemical yield
SSTR2	Somatostatin receptor type II
THP	Tris(3-hydroxypyridin-4-one)
THPO	Tris(6-methyl-3-hydroxypyran-4-one)

Conflicts of interest

P. J. B. and R. C. H. are named inventors on related patents. All other authors have no conflicts to declare.

Acknowledgements

We acknowledge support from KCL and UCL Comprehensive Cancer Imaging Centre funded by CRUK and EPSRC in association with the MRC and DoH (England) and Medical Engineering Centre at King's College London funded by the Wellcome Trust and EPSRC (203148/Z/16/Z)). Cinzia Imberti was supported by a PhD studentship funded by the NIHR Biomedical Research Centre award to Guy's and St Thomas' NHS Foundation Trust in partnership with King's College London and King's College Hospital NHS Foundation Trust. Jennifer D. Young was funded by the King's College London and Imperial College London EPSRC Centre for Doctoral Training in Medical Imaging (EP/L015226/1) and Theragnostics Limited. Brett Paterson was supported by a Victorian Postdoctoral Research Fellowship funded by the Victorian Government, Australia. PET scanning equipment was funded by an equipment grant from the Wellcome Trust. No other potential conflict of interest relevant to this article was reported.

Authors contribution

All authors have given approval to the final version of the manuscript.

Abbreviations

CT	Computed tomography
DCC	Dicyclohexylcarbodiimide
EDTA	Ethylenediaminetetraacetic acid
FSC	Fusarinine-C
HBED	<i>N,N</i> -Bis(2-hydroxybenzyl)ethylenediamine- <i>N,N</i> -diacetic acid
HOBT	Hydroxybenzotriazole
HP	3-Hydroxypyridin-4-one
HPLC	High performance liquid chromatography
iTLC-SG	Instant thin-layer chromatography-silica gel
MIP	Maximum intensity projection

References

- 1 I. Velikyan, *J. Labelled Compd. Radiopharm.*, 2015, **58**, 99–121.
- 2 I. Velikyan, *Theranostics*, 2013, **4**, 47–80.
- 3 M. D. Bartholoma, A. S. Louie, J. F. Valliant and J. Zubieta, *Chem. Rev.*, 2010, **110**, 2903–2920.
- 4 I. Velikyan, *Med. Chem.*, 2011, **7**, 345–379.
- 5 A. Afshar-Oromieh, A. Malcher, M. Eder, M. Eisenhut, H. G. Linhart, B. A. Hadaschik, T. Holland-Letz, F. L. Giesel, C. Kratochwil, S. Haufe, U. Haberkorn and C. M. Zechmann, *Eur. J. Nucl. Med. Mol. Imaging*, 2013, **40**, 486–495.
- 6 A. Afshar-Oromieh, C. M. Zechmann, A. Malcher, M. Eder, M. Eisenhut, H. G. Linhart, T. Holland-Letz, B. A. Hadaschik, F. L. Giesel, J. Debus and U. Haberkorn, *Eur. J. Nucl. Med. Mol. Imaging*, 2014, **41**, 11–20.
- 7 P. J. Blower, *Dalton Trans.*, 2015, **44**, 4819–4844.



- 8 E. W. Price and C. Orvig, *Chem. Soc. Rev.*, 2014, **43**, 260–290.
- 9 B. M. Zeglis, J. L. Houghton, M. J. Evans, N. Viola-Villegas and J. S. Lewis, *Inorg. Chem.*, 2013, **54**, 1880–1899.
- 10 J. Simecek, M. Schulz, J. Notni, J. Plutnar, V. Kubicek, J. Havlickova and P. Hermann, *Inorg. Chem.*, 2012, **51**, 577–590.
- 11 J. Notni, J. Simecek, P. Hermann and H.-J. Wester, *Chem. – Eur. J.*, 2011, **17**, 14718–14722.
- 12 B. P. Waldron, D. Parker, C. Burchardt, D. S. Yufit, M. Zimny and F. Roesch, *Chem. Commun.*, 2013, **49**, 579–581.
- 13 J. Seemann, B. P. Waldron, F. Roesch and D. Parker, *ChemMedChem*, 2015, **10**, 1019–1026.
- 14 A. Vagner, A. Forgacs, E. Brucher, I. Toth, A. Maiocchi, A. Wurzer, H. J. Wester, J. Notni and Z. Baranyai, *Front. Chem.*, 2018, **6**, 1–12.
- 15 J. Simecek, P. Hermann, H. J. Wester and J. Notni, *ChemMedChem*, 2013, **8**, 95–103.
- 16 E. Farkas, J. Nagel, B. P. Waldron, D. Parker, I. Toth, E. Brucher, F. Rosch and Z. Baranyai, *Chem. – Eur. J.*, 2017, **23**, 10358–10371.
- 17 E. Boros, C. L. Ferreira, J. F. Cawthray, E. W. Price, B. O. Patrick, D. W. Wester, M. J. Adam and C. Orvig, *J. Am. Chem. Soc.*, 2010, **132**, 15726–15733.
- 18 R. D. Shannon, *Acta Crystallogr., Sect. A: Cryst. Phys., Diffraction, Theor. Gen. Crystallogr.*, 1976, **32**, 751–767.
- 19 C. Y. Zhai, D. Summer, C. Rangger, H. Haas, R. Haubner and C. Decristoforo, *J. Labelled Compd. Radiopharm.*, 2015, **58**, 209–214.
- 20 C. Caraco, L. Aloj and W. C. Eckelman, *Appl. Radiat. Isot.*, 1998, **49**, 1477–1479.
- 21 M. I. Tsonou, C. E. Knapp, C. A. Foley, C. R. Munteanu, A. Cakebread, C. Imberti, T. R. Eykyn, J. D. Young, B. M. Paterson, P. J. Blower and M. T. Ma, *RSC Adv.*, 2017, **7**, 49586–49599.
- 22 M. Eder, M. Schaefer, U. Bauder-Wuest, W.-E. Hull, C. Waengler, W. Mier, U. Haberkorn and M. Eisenhut, *Bioconjugate Chem.*, 2012, **23**, 688–697.
- 23 R. J. Motekaitis, Y. Sun, A. E. Martell and M. J. Welch, *Inorg. Chem.*, 1991, **30**, 2737–2740.
- 24 D. J. Berry, Y. Ma, J. R. Ballinger, R. Tavaré, A. Koers, K. Sunassee, T. Zhou, S. Nawaz, G. E. D. Mullen, R. C. Hider and P. J. Blower, *Chem. Commun.*, 2011, **47**, 7068–7070.
- 25 M. T. Ma, L. K. Meszaros, B. M. Paterson, D. J. Berry, M. S. Cooper, Y. Ma, R. C. Hider and P. J. Blower, *Dalton Trans.*, 2015, **44**, 4884–4900.
- 26 M. T. Ma, C. Cullinane, K. Waldeck, P. Roselt, R. J. Hicks and P. J. Blower, *EJNMMI Res.*, 2015, **5**, 52.
- 27 M. T. Ma, C. Cullinane, C. Imberti, J. Baguna Torres, S. Y. A. Terry, P. Roselt, R. J. Hicks and P. J. Blower, *Bioconjugate Chem.*, 2016, **27**, 309–318.
- 28 J. D. Young, V. Abbate, C. Imberti, L. K. Meszaros, M. T. Ma, S. Y. A. Terry, R. C. Hider, G. E. Mullen and P. J. Blower, *J. Nucl. Med.*, 2017, **58**, 1270–1277.
- 29 C. Imberti, S. Y. A. Terry, C. Cullinane, F. Clarke, G. H. Cornish, N. K. Ramakrishnan, P. Roselt, A. P. Cope, R. J. Hicks, P. J. Blower and M. T. Ma, *Bioconjugate Chem.*, 2017, **28**, 481–495.
- 30 M. S. Hofman, P. Eu, P. Jackson, E. Hong, D. Binns, A. Irvani, D. Murphy, C. Mitchell, S. Siva, R. J. Hicks, J. D. Young, P. J. Blower and G. E. Mullen, *J. Nucl. Med.*, 2018, **59**, 625–631.
- 31 D. Lobeek, G. M. Franssen, M. T. Ma, H.-J. Wester, C. Decristoforo, W. J. G. Oyen, O. C. Boerman, S. Y. A. Terry and M. Rijpkema, *J. Nucl. Med.*, 2018, **59**, 1296–1301.
- 32 T. Zhou, H. Neubert, D. Y. Liu, Z. D. Liu, Y. M. Ma, X. L. Kong, W. Luo, S. Mark and R. C. Hider, *J. Med. Chem.*, 2006, **49**, 4171–4182.
- 33 R. Cusnir, C. Imberti, R. C. Hider, P. J. Blower and M. T. Ma, *Int. J. Mol. Sci.*, 2017, **18**, 116.
- 34 S. Nawaz, G. E. D. Mullen, K. Sunassee, J. Bordoloi, P. J. Blower and J. R. Ballinger, *EJNMMI Res.*, 2017, **7**, 86.
- 35 T. Derlin, S. Schmuck, C. Juhl, S. Teichert, J. Zörgiebel, H.-J. Wester, S. M. Schneefeld, A. C. A. Walte, J. T. Thackeray, T. L. Ross and F. M. Bengel, *Mol. Imaging Biol.*, 2018, **20**, 650–658.
- 36 T. Derlin, S. Schmuck, C. Juhl, J. Zörgiebel, S. M. Schneefeld, A. C. A. Walte, K. Hueper, C. A. von Klot, C. Henkenberens, H. Christiansen, J. T. Thackeray, T. L. Ross and F. M. Bengel, *Eur. J. Nucl. Med. Mol. Imaging*, 2018, **45**, 913–922.
- 37 G. Cook, S. Hughes, S. Morris, B. Challacombe, P. Cathcart, R. Popert, C. Brown, P. Dasgupta, J. John, A. Mallia, J. Young, V. Gibson, G. Mullen and V. Warbey, British Nuclear Medicine Society 46th Annual Spring Meeting, 2018, vol. 39, p. 50.
- 38 P. S. Dobbin, R. C. Hider, A. D. Hall, P. D. Taylor, P. Sarpong, J. B. Porter, G. Y. Xiao and D. Vanderhelm, *J. Med. Chem.*, 1993, **36**, 2448–2458.
- 39 Z. D. Liu, R. Kayyali, R. C. Hider, J. B. Porter and A. E. Theobald, *J. Med. Chem.*, 2002, **45**, 631–639.
- 40 R. C. Hider and Z. D. Liu, *Curr. Med. Chem.*, 2003, **10**, 1051–1064.
- 41 S. Piyamongkol, Y. M. Ma, X. L. Kong, Z. D. Liu, M. D. Aytemir, D. van der Helm and R. C. Hider, *Chem. – Eur. J.*, 2010, **16**, 6374–6381.
- 42 B. L. Rai, L. S. Dekhordi, H. Khodr, Y. Jin, Z. D. Liu and R. C. Hider, *J. Med. Chem.*, 1998, **41**, 3347–3359.
- 43 Y. Y. Xie, Z. D. Lu, X. L. Kong, T. Zhou, S. Bansal and R. Hider, *Eur. J. Med. Chem.*, 2016, **115**, 132–140.
- 44 S. R. Vallabhajosula, J. F. Harwig, J. K. Siemsen and W. Wolf, *J. Nucl. Med.*, 1980, **21**, 650–656.
- 45 P. D. Taylor, *Talanta*, 1995, **42**, 845–850.
- 46 J. Notni, P. Hermann, J. Havlickova, J. Kotek, V. Kubicek, J. Plutnar, N. Loktionova, P. J. Riss, F. Roesch and I. Lukes, *Chem. – Eur. J.*, 2010, **16**, 7174–7185.
- 47 P. Gans and B. O'Sullivan, *Talanta*, 2000, **51**, 33–37.
- 48 P. Gans, A. Sabatini and A. Vacca, *Talanta*, 1996, **43**, 1739–1753.



- 49 P. Gans, A. Sabatini and A. Vacca, *Ann. Chim.*, 1999, **89**, 45–49.
- 50 E. A. Martell and R. M. Smith, *Critical Stability Constants*, Plenum Press, New York, 1977–1989.
- 51 L. Alderighi, P. Gans, A. Ienco, D. Peters, A. Sabatini and A. Vacca, *Coord. Chem. Rev.*, 1999, **184**, 311–318.
- 52 I. Szanda, J. Mackewn, G. Patay, P. Major, K. Sunassee, G. E. Mullen, G. Nemeth, Y. Haemisch, P. J. Blower and P. K. Marsden, *J. Nucl. Med.*, 2011, **52**, 1741–1747.
- 53 M. Magdics, L. Szirmay-Kalos, B. Toth, D. Legrady, A. Cserkaszky, L. Balkay, B. Domonkos, D. Voelgyes, G. Patay, P. Major, J. Lantos and T. Buekki, 2011 Ieee Conference (Nss/Mic), 2011, pp. 4086–4088.

